Quantification of oxidative stress phenotypes based on high-throughput growth profiling of protein kinase and phosphatase knockouts

Altnta, Ali; Martini, Jacopo; Mortensen, Uffe Hasbro; Workman, Christopher T.

Published in:
FEMS Yeast Research

Link to article, DOI:
10.1093/femsyr/fov101

Publication date:
2016

Document Version
Publisher's PDF, also known as Version of record

FEMS Yeast Research, 16, 2016, fov101

doi: 10.1093/femsyr/fov101
Advance Access Publication Date: 11 November 2015
Research Article

RESEARCH ARTICLE

Quantification of oxidative stress phenotypes based on high-throughput growth profiling of protein kinase and phosphatase knockouts

Ali Altıntaş[1], Jacopo Martini[1], Uffe H. Mortensen[2] and Christopher T. Workman[1,*]

[1]Center for Biological Sequence Analysis, Department of Systems Biology, Technical University of Denmark, Building 208, Kongens Lyngby, DK-2800, Denmark and [2]Eukaryotic Biotechnology, Department of Systems Biology, Technical University of Denmark, Building 223, Kongens Lyngby, DK-2800, Denmark

*Corresponding author: Center for Biological Sequence Analysis, Department of Systems Biology, Technical University of Denmark, Kemitorvet bld 208, Kgs. Lyngby, DK-2800, Denmark. Tel: +45 4525 2477; E-mail: workman@cbs.dtu.dk

One sentence summary: The dynamics of dosage-dependent oxidative stress response revealed complex phenotypic profiles in a comprehensive set of protein kinases and phosphatases.

Editor: Jens Nielsen

ABSTRACT

Cellular responses to oxidative stress are important for restoring redox balance and ensuring cell survival. Genetic defects in response factors can lead to impaired response to oxidative damage and contribute to disease and aging. In single cell organisms, such as yeasts, the integrity of the oxidative stress response can be observed through its influences on growth characteristics. In this study, we investigated the time-dependent batch growth effects as a function of oxidative stress levels in protein kinase and phosphatase deletion backgrounds of *Saccharomyces cerevisiae*. In total, 41 different protein kinases and phosphatase mutants were selected for their known activities in oxidative stress or other stress response pathways and were investigated for their dosage-dependent response to hydrogen peroxide. Detailed growth profiles were analyzed after the induction of stress for growth rate, lag time duration and growth efficiency, and by a novel method to identify stress-induced diauxic shift delay. This approach extracts more phenotypic information than traditional plate-based methods due to the assessment of time dynamics in the time scale of minutes. With this approach, we were able to identify surprisingly diverse sensitivity and resistance patterns as a function of gene knockout.

Keywords: oxidative stress; growth physiology; fitness; systems biology; protein kinase; protein phosphatase

INTRODUCTION

Reactive oxygen species (ROS) have been linked to aging and a variety of diseases in higher eukaryotes, such as cancer, neurodegenerative and cardiovascular disease (Ames, Shigenaga and Hagen 1993; Halliwell 1997; Temple, Perrone and Dawes 2005; Farrugia and Balzan 2012). ROS formation is primarily generated by the mitochondrial electron transport chain activity of the cell during aerobic respiration (Perrone, Tan and Dawes 2008) and, as such, their formation is unavoidable. The wide array of detrimental effects of ROS on human health is due to their ability to react with and damage many different cellular components especially DNA (Cooke *et al.* 2003), proteins (Nystrom 2005) and lipids (Herdeiro *et al.* 2006; Landolfo *et al.* 2010) by triggering 8-oxoguanine formation (van Loon, Markkanen and Hubscher

Received: 21 May 2015; **Accepted:** 8 November 2015

2010), protein carbonylation (Nystrom 2005) and lipid peroxidation (Howlett and Avery 1997), respectively. To cope with this, eukaryotic cells have developed many different mechanisms to respond to ROS-induced damage. This includes systems for sensing, signaling and activating repair mechanisms. For example, 8-oxoguanines are removed from DNA by Ogg1p catalyzed base excision repair (Singh *et al*. 2001), carbonylated proteins are tagged for proteasomal degradation (Nystrom 2005) and lipid peroxides are removed by phospholipid-hydroperoxide glutathione peroxidase (e.g. Gpx1p) (Avery and Avery 2001). The high osmolarity glycerol (HOG) pathway signals salt stress via mitogen-activated protein kinases (Singh 2000; Ikner and Shiozaki 2005) but also activates AP-1 like transcription factors (e.g. Yap1p) (Ikner and Shiozaki 2005) which are known to regulate oxidative stress responses.

The response to oxidative stress differs according to the level of the stress. When cells are exposed to low levels of oxidants, an adaptive response is frequently initiated, which results in a transient resistance to higher levels of stress (Jamieson 1998); on the other hand high levels of oxidants can cause cell cycle delay allowing time for antioxidant synthesis as well as for induction and use of the relevant repair systems (Hohmann and Mager 2003). Taking advantage of budding yeasts amenability to genetic engineering, this phenomenon has been studied intensively in the budding yeast *Saccharomyces cerevisiae* (Jamieson 1992; Jamieson 1998; Ng *et al*. 2008). Hence, genome-wide mutant collections have been analyzed for relevant phenotypes, including sensitivity and resistance to oxidative stress, typically using assays based on growth on solid medium. In this manner, many genes (Huang *et al*. 2003; Huang and Kolodner 2005; Paumi *et al*. 2012) have been linked to oxidative stress response and damage repair, although primarily in assays on solid medium.

Exposure to alkylating agents, such as methyl methanesulfonate (MMS), is also known to generating ROS in addition to damaging DNA. Thus, the oxidative stress response is related to the DNA damage response (Salmon *et al*. 2004; Kitanovic and Wolfl 2006). Furthermore, the toxicity caused by the oxidants and alkylating agents is dependent on the concentration of glucose in the growth medium (Osorio *et al*. 2004; Zong *et al*. 2004). ROS formation creates a response, which modulates glucose metabolism and consequently, increases the survival ratio of the MMS-treated cells (Kitanovic and Wolfl 2006).

Although the growth physiology of *S. cerevisiae* has been well characterized, it is surprising that oxidative stress responses have only been analyzed to a limited extent during submerged cultivation. For typical batch cultivations of *S. cerevisiae* in nutrient-rich media, cells grow exponentially up to the exhaustion of glucose, the primary carbon source. Metabolism is then reprogrammed during the *diauxic shift* (Monod 1949; Winderickx *et al*. 2003), a phase where cells prepare to consume secondary carbon sources such as ethanol produced during glucose consumption as a result of the Crabtree effect (De Deken 1966). When all carbon sources in the surrounding media are consumed, cells enter stationary phase (Hohmann and Mager 2003). During the diauxic shift, cell size and all metabolic events related to energy metabolism are directly affected by redirection of carbon flux from fermentative pathway to respiratory pathway (Brauer *et al*. 2005, 2008). Growth physiology parameters, such as growth rate (Blomberg 2011), diauxic shift times and lag phase delay, are important parameters of cellular fitness. Importantly, as energy metabolism changes during the diauxic shift to aerobic respiration, ROS production is increased, which elicits an oxidative challenge (Gasch *et al*. 2000). Therefore, by examining growth physiology of submerged cultivations as a phenotypic trait during oxidative damage, novel links between genotypes and phenotypes may be uncovered to increase our understanding of the oxidative stress response.

To gain insight into how the oxidative stress response influences the overall growth physiology of *S. cerevisiae*, we systematically analyzed yeast deletion mutants for important cell signaling factors, protein kinases and phosphatases, to measure their effects on four key parameters that characterize growth during batch fermentations in the presence or absence of oxidative stress. Gene deletions were selected for their known effects in oxidative and DNA damage responses to ensure a representative set of protein kinases and phosphatases (Kelley and Ideker 2009; Cherry *et al*. 2012). In addition, knockouts of genes encoding protein kinases and phosphatases that play roles in other well-known pathways, such as actin cytoskeleton regulation (ACR), cell cycle control (CC), carbon metabolism (CM), cell wall integrity (CWI), DNA damage response (DDR), exocytosis regulation (EXO), high osmolarity glycerol (HOG), target of rapamycin (TOR) and vacuolar protein sorting (VPS), were also investigated. Physiological parameters were then analyzed to identify potential differences in response pattern due to the mutant background. Based on our analyses, we identified mutant strains that were significantly more sensitive or resistant to oxidative stress when compared to the reference strains and growth condition. The relative phenotypes were clustered into different phenotypic profiles, which were then used to identify both established and novel links between genes and response to oxidative stress. Importantly, the phenotypic patterns of five parologous protein kinase pairs were analyzed for their similarities or differences. Moreover, this led us to identify the fitness variability of paralogous pairs in larger datasets.

MATERIALS AND METHODS

Yeast strains and growth conditions

An effort was made to study a representative set of stress-related protein kinases and phosphatases via their single gene deletion strains. Basically, these representative genes were consisted of two groups: well-known stress signaling pathways (HOG, CWI, DDR) and stress-related regulatory pathways [TOR, CC, VPS, ACR, CM, EXO and SW (spore wall biogenesis)]. In total, we obtained the 41 stress-related protein kinase (34) and phosphatase (7) knockout strains derived from closely related strain backgrounds (isogenic derived from S288c): BY4741, Y7220 and Y7092 from the Matthias Peter and Ruedi Aebersold labs (Bodenmiller *et al*. 2010) (see Table S1, Supporting Information).

There are 159 PK/PPs in *S. cerevisiae* (Breitkreutz *et al*. 2010), ~19% of them ($n = 31$) were reported to cause a phenotype in oxidative stress (sensitivity or resistance) according to Saccharoymces Genome Database (SGD). With this knowledge, we selected a representative set of 13 of these 31 genes with known oxidative stress response phenotypes expecting that >40% of the known examples would be representative of the possible phenotypic patterns. The remaining 28 were selected for their relevance to other stress responses. For example, genes were also selected from HOG (4), CWI (3), CC (2) as well as single examples from DDR, TOR, ACR and SW pathways (as defined by SGD) in an effort to define a representative set of stress-related PKs and PPs that were not believed to be oxidative stress related. Other PK/PP genes were added as irrelevant controls such as Δ*vps15*, Δ*yck3*, Δ*pkp1*, Δ*yck1* and Δ*kin1*. A detailed overview of reported oxidative stress phenotypes and the strains

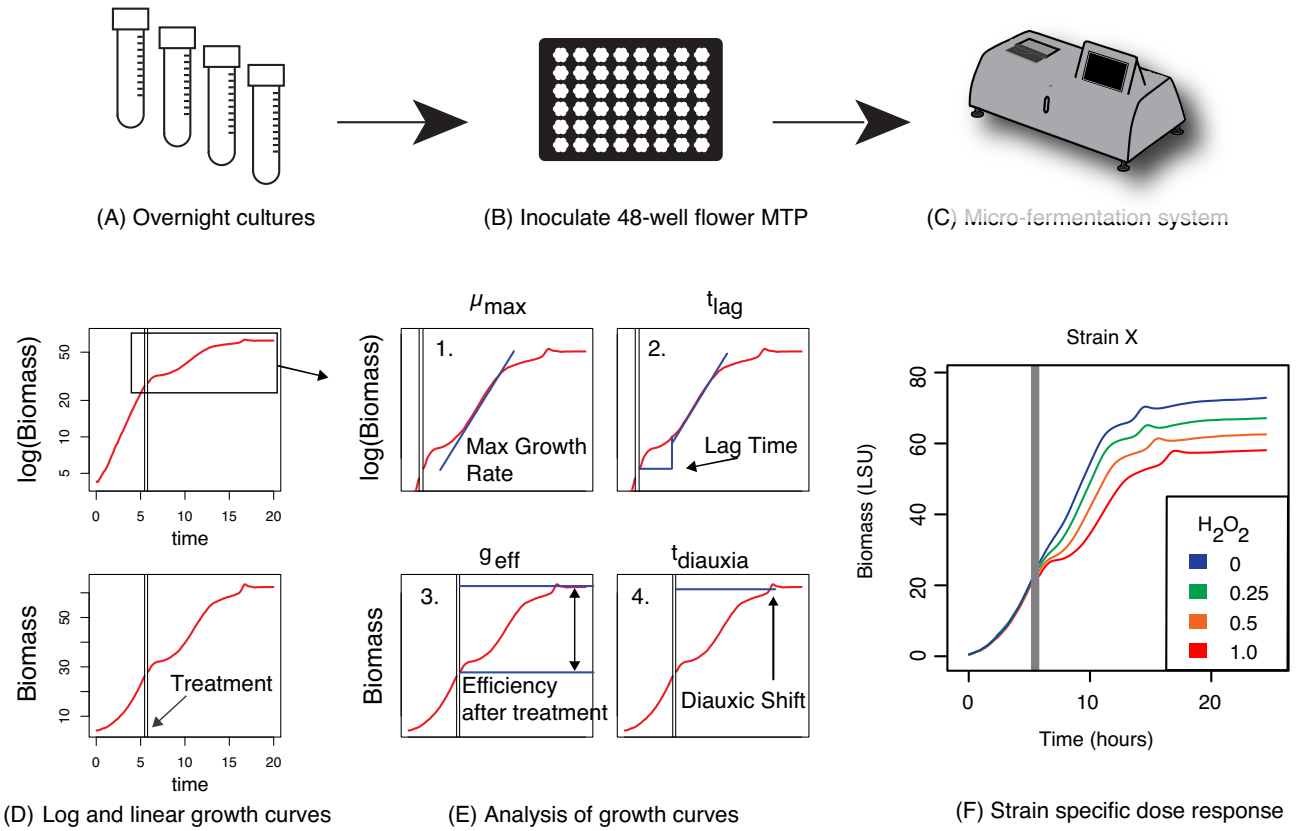

Figure 1. Experimental overview for strain fitness quantification. The strains were inoculated overnight (**A**) and transferred to 48 flower-well microtiter plates (starting OD_{600} was 0.2) for batch fermentations (**B** and **C**). The treatments with H_2O_2 were performed at mid-log phase and data acquired from each well every 3 minutes (**D**). Downstream data analyses were performed to extract the growth properties: (1) maximum growth rate (μ-max), (2) lag time (t-lag), (3) growth efficiency (g-eff) and (4) diauxic shift time (t-diauxie) (**E**). Strain-specific dose response can be seen in the last panel (**F**) when the inoculum was treated with varying concentrations of H_2O_2.

selected in this study can be found in Table S2 (Supporting Information).

Cell stocks in 15% glycerol containing YPD (1% yeast extract, 2% glucose, 2% peptone and 2% Bacto-agar for agar plates-) taken from −80°C were thawed and streaked on YPD agar plates. YPD agar plates were incubated at 30°C up to 2–3 days.

Growth physiology and the time dynamics of the stress response were characterized in a microfermentation system (BioLector, m2p-Labs) for all deletion strains, Fig. 1A–C. After 24 hours incubation of the precultures, the OD_{600} was measured by NanoDrop 1000. An initial OD_{600} of 0.2 was achieved for each sample by dilution in synthetic defined medium (SD medium: 1.7 g L^{-1} yeast nitrogen base without amino acids, 5 g L^{-1} ammonium sulfate, 20 g L^{-1} dextrose, 1.325 g L^{-1} Brent Supplement Mixture (Saghbini, Hoekstra and Gautsch 2001) with 0.1 mg L^{-1} L-Leucine). The samples were then transferred into the 48-well BioLector flower plates (m2p-Labs, MTP-48-B). The plates are sealed with gas permeable adhesive seals (Thermo, AB-0718) after transfer into the wells. Batch growth of cell populations was measured at 620 nm scattered light by BioLector. All strains, except Δ*vps15* (where the initial OD was set to 0.4 OD due to slow growth), reached the mid-log phase at ∼5.5 hours where the cells were treated with H_2O_2 (Sigma, H1009) to final concentrations of 0.25, 0.5 and 1.0 mM. The BioLector cultivations continued to 36 hours or more and all microfermentation experiments were performed at least twice as biological replicates. The same procedure was followed for MMS (Sigma, M4016) treatments with 0.05% (v/v) concentration.

Determination of metabolite contents by HPLC

Reference strain, BY4741, was inoculated and cultivation in BioLector started at 0.2 absorbance of OD_{600}. The sampling times were determined as: *t0*, initial inoculum; *t1*, pre-treatment (∼5.5 hours) in mid-log phase; *t2*, pre-diauxic shift; *t3*, post-diauxic shift; and *t4*, stationary phase (∼36 hours).

Sampling was done by taking 1 ml of cells and media away from the flower plate wells with a syringe and filtering it using 0.45 μm filters (MiniStart-plus, Sartorius) to the HPLC vials (Supelco). HPLC analysis was then performed with 20 μl injection from these samples. An isocratic method was run at 60°C with 0.6 ml $minute^{-1}$ flow rate of 5 mM sulfuric acid (BioRad, Aminex HPX-87H). Metabolite compositions were determined by comparison to retention time (RT) with UV absorbance (UV) and refractive index (RI) signal for six known standards: glucose (RT = 9.28 minutes, by RI), pyruvate (RT = 9.40 minutes, by UV), succinate (RT = 11.53 minutes, by RI), glycerol (RT = 13.53 minutes, by RI), acetate (RT = 14.88 minutes, by UV; RT = 15.13 minutes, by RI) and ethanol (RT = 22.65 minutes, by RI).

Data analysis

The R Statistical Programming Language (version R-3.0.2) was used for analyzing all data sets. There were four characteristics used for the analysis of strain-specific growth profiles: maximum growth rate (μ-max); lag-phase duration (t-lag); efficiency of growth (g-eff) 24 hours after treatment with H_2O_2;

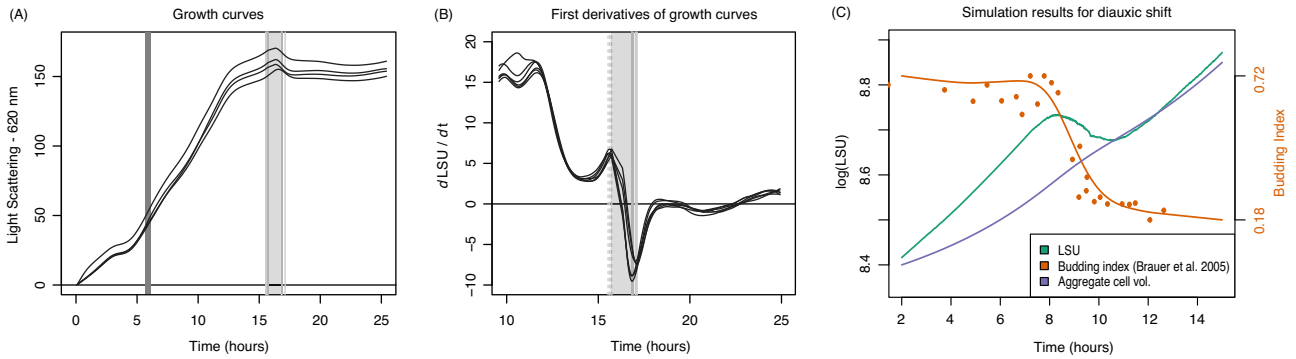

Figure 2. Diauxic shift detection based on the first derivatives of example growth curve replicates. (**A**) A typical growth curve generated by BioLector microfermentation platform. (**B**) First derivatives of the growth curves (dy/dt) are in terms of change in LSU per change in time (hours). Dashed vertical lines indicate the maximum dy/dt, while straight lines indicate the minimum dy/dt in the diauxic shift. Shaded regions represent the same diauxic phase in both A and B. (**C**) Simulation results showing predicted fluctuations in light-scattering profile (green) due to rapid changes in budding index as was observed in Brauer *et al.* (2005) (orange). The budding index measures (orange points) and smoothing spline (orange curve) were used to simulate release of buds from mother cells. All cells were simulated to grow at a constant rate giving a monotone increase in aggregate cell volume (blue).

and diauxic-shift delay times (t-diauxie) as shown in Fig. 1E. The maximum growth rate (μ) (the biggest change in log of biomass per unit time) was estimated at the time window between 1 and 3 hours after treatment with either H_2O_2 or MMS as the maximum slope of the growth curve (Equation 1).

$$\forall i \in (0,\ 3) \Rightarrow \mu_{\max} = \frac{d\left(\log\left(y\right)\right)}{dt} \tag{1}$$

where i was the time window for μ-max detection, y was biomass in light-scattering units (LSU) and t was time in hours.

t-lag is estimated based on a modification of the approach of Monod in 1949 (also illustrated in Fig. 1E-2) due to the observed delay in onset of growth inhibition. To account for this, we find the first time point where the deviation is at most 10% of the maximum deviation from the linear fit, i.e. $\max(|y_{\text{fit}} - y|) \times 0.1$. g-eff is calculated by Equation (2):

$$g_{\text{eff}} = y_{t+24} - y_t \tag{2}$$

where g-eff represented growth efficiency, y indicated the biomass in LSU and t indicated time in hours.

Detection of diauxic shift phase

The diauxic shift time intervals were detected by using the first derivatives (dy/dt) of the growth curves since diauxie has a unique signature on the growth curve in this phase. Once the slope of the growth curve reaches a minimum negative value following a local maximum, that time interval was used to define the diauxic phase interval (Fig. 2).

To demonstrate a relationship between light-scattering changes in the diauxic shift and the fraction of budded cells in liquid cell culture, we have performed a simple growth simulation for 1000 cell particles (budded + free cells) that follows the budding index profile from Brauer *et al.* (2005). We have conservatively estimated the diameter of budded cells as the mean of the long axis (sum of mother and daughter diameters) and the short axis (mean of mother and daughter diameters). The diameter (μm) of the mother and free cells were drawn from a normal distribution, $N(\text{m} = 5, \text{s} = 0.5)$, while the buds were drawn from $N(\text{m} = 3.5, \text{s} = 0.5)$. A 0.1% bud growth was applied at each time step. Light-scattering intensity was estimated by Rayleigh scattering (Cox, DeWeerd and Linden 2002) integrated over all free particles in solution (see Equation 3),

$$I \sim {}^{d^6}\!/_{\lambda^4} \tag{3}$$

where d is the diameter in μm and λ is the light wavelength (a constant 620 nm). At each step, a sufficient number of budded cells were selected at random and separated in order to match the smoothed budding index curve of Brauer *et al.* (2005).

Hierarchical clustering

Based on the four different measures estimated from each individual growth profile, the relative oxidative stress responses were calculated for each criterion as shown in Equation (4).

$$\Delta\tau^{\text{HP}}_{i,j,k} = f\left(\tau_{i,j,k} - \tau_{i,j,0}\right)\phi_i$$
$$f\left(x\right) = \frac{x}{\sigma} \tag{4}$$

where $\tau_i = \{\mu_{\max}, t_{\text{lag}}, g_{\text{eff}}, t_{\text{diauxia}}\}$ indicates the growth properties, j indicates the strains and $k = \{0,\ 0.25,\ 0.5,\ 1\}$ indicates the treatment conditions, respectively. Since the ranges of the measures differed, relative measures were scaled to $\Delta\tau$ by dividing by their standard deviation. Since negative values of t-diauxie and t-lag represented resistance, i.e. a positive trait, these values were negated to provide fitness measures using $\phi_i = \{1,\ -1,\ 1,\ -1\}$, corresponding to the four growth parameters, τ_i.

After calculating each $\Delta\tau^{\text{HP}}_{i,j,k}$, a matrix was generated for hierarchical clustering (Eisen *et al.* 1998). In addition to this analysis, we analyzed the effects of the deleted gene. Thus, reference strain backgrounds were subtracted from their relevant knockout strains (Equation 5).

$$\Delta\tau^{\text{BG}}_{i,j,k} = f\left(\tau_{i,j,k} - \tau_{i,\text{BG}_j,k}\right)\phi_i \tag{5}$$

where BG_j stands for the reference background of strain j (the other variables are the same of Equation 4).

For the final analysis, defined in Equation (6), we subtracted both no-treatment control (Equation 4) and strain background

(Equation 5) together. In this sense, the negative values would correspond to strain sensitivity whereas positive values indicate strain resistance.

$$\Delta\tau^{\mathrm{rel}}_{i,j,k} = \left(\Delta\tau^{\mathrm{HP}}_{i,j,k} - \Delta\tau^{\mathrm{HP}}_{i,\mathrm{BG}_j,k}\right)\phi_i \quad (6)$$

After calculating individual τ values, we have applied a generalized linear model per strain and calculated interaction term t-statistics (see below). The t-values were then transformed as described in Equation (4) to describe the patterns of each fitness parameter. Finally, hierarchical clustering was applied to the resulting matrix using the complete linkage method and the Euclidian distance.

T-statistics

A generalized linear model was applied to $\Delta\tau^{\mathrm{rel}}_{i,j}$ for all data from each knockout versus all background data. The model was defined (using the *glm* function in R with model y $\sim s \times h$, where *y* is the relative response, *s* is the knockout status {0,1} and *h* is the hydrogen peroxide level) to estimate the influence of the deleted gene, the peroxide treatment level and the interaction of the two. Equation (7) describes the generalized linear model approach we used:

$$\Delta\tau^{\mathrm{rel}} = \beta_0 + \beta_1 s + \beta_2 h + \beta_3 sh \quad (7)$$

where β_0 is an offset, β_1 is the knockout effect term (*s*), β_2 is the hydrogen peroxide affect term (*h*) and $\beta_3$is the interaction term (*sh*).

We extracted the t-values and p-values from these models to summarize the fitness properties of each growth parameter. Of particular interest was the t-statistic value for the interaction term (β_3), which was related to the slope of $\Delta\tau^{\mathrm{rel}}_{i,j}$ versus peroxide concentration and, therefore, a direct measure of the knockout's relative dose response. The p-values were adjusted by the Benjamini and Hochberg method (1995).

Comparison of background strains

Each of the four growth parameters was tested for the influence of the background strain under varying H_2O_2 treatments by applying two-way ANOVA test. Thereafter, ANOVA model was processed with Tukey's HSD (honest significance test) with 95% confidence interval as a post-hoc significance test to calculate the pairwise p-values of interaction between background strains and H_2O_2 treatments.

K-means clustering of external data

The fitness data from PROPHECY database (Fernandez-Ricaud *et al.* 2005) were retrieved and all available catalytic kinases and phosphatases (Breitkreutz *et al.* 2010) were selected from the dataset.

The number of k-means clusters was detected by using Bayesian Information Criterion statistics, and a 'goodness of fit' criterion, which selects the model with smallest K (Jombart 2008). The paralogy information was retrieved from SGD (Cherry *et al.* 2012). Finally, paralogous gene pairs were analyzed for their cluster membership (same versus different cluster). The empirical p-values were calculated for paralogous pairs by permuting the cluster assignment 10^5 times and counting the number of paralogs in the same cluster each trial.

Comparison to external data

The paraquat and diamide treatment data from PROPHECY database were retrieved and protein kinase/phosphatase knockouts used in this study were identified. The data from our study were converted to logarithmic phenotypic indices (LPI) (Warringer *et al.* 2003) for a proper comparison. The other datasets were retrieved from microarray-based competitive growth assays, and log-fold changes were used as a comparison criterion (Parsons *et al.* 2006; Kelley and Ideker 2009; Hillenmeyer *et al.* 2010). The correlation among these different data types was determined by Spearman correlation and the p-values of this correlation were adjusted by the Benjamini and Hochberg method (1995).

HPLC metabolite concentrations

Calibration curves were fit using cubic splines (due to nonlinearity) to integrated peak areas over six standard concentrations for each metabolite. Metabolite concentrations in each sample were estimated according to these calibration curves (data not shown).

Glucose, glycerol and ethanol amounts per treatment were compared to each other when the cells were about to enter diauxic shift. The time points closest prior to diauxic shift corresponded to 15.8 hours for 0, 0.25 and 0.5 mM H_2O_2 treatments and 25.6 hours for 1 mM treatment. The difference between each series of metabolites was tested by pairwise t-test and the p-values were adjusted by the Benjamini and Hochberg method (1995).

RESULTS

Diauxic shift has a distinctive light-scattering signature

In this study, we have utilized a microfermentation system that allows for growth profiling of 44 strains in parallel, see Fig. 1A–C. To characterize this setup, we first determined the growth curves for the reference strains in SD medium (Fig. 1D). In each case, a characteristic and reproducible light-scattering signature was observed in the growth curves at the transition between two distinct growth phases, which we speculated represented the diauxic shift. To confirm this, a batch fermentation of *S. cerevisiae* BY4741 was performed, tracked online and sampled for HPLC analysis at the time of this signature as indicated in Fig. 3A.

Analysis of glucose levels indicated that these signatures coincide or directly follow the exhaustion of glucose, and thus mark the diauxic phase (Fig. 3B). In agreement with this, ethanol production increased during the first exponential growth phase up to the signature but decreased shortly after (Fig. 3C) confirming the consumption of ethanol after the diauxic phase as expected. Similarly, other indicators of diauxic shift, glycerol and pyruvate (Fig. 3D and F) also increased up to the end of first exponential growth, at which point the concentration of pyruvate quickly dropped while glycerol remained constant. In contrast, acetate production, which is produced during aerobic metabolism of both glucose and ethanol, increased over the entire batch growth (Fig. 3E). Acetate is known to be produced during growth on glucose but its production is dependent on NADH+ concentration (Pons, Rajab and Engasser 1986). The continued production of acetate during our batch fermentations indicates that NADH+ levels were sufficient.

Glycerol levels were examined at the time points closest to the diauxic shift for each treatment level as can be seen in

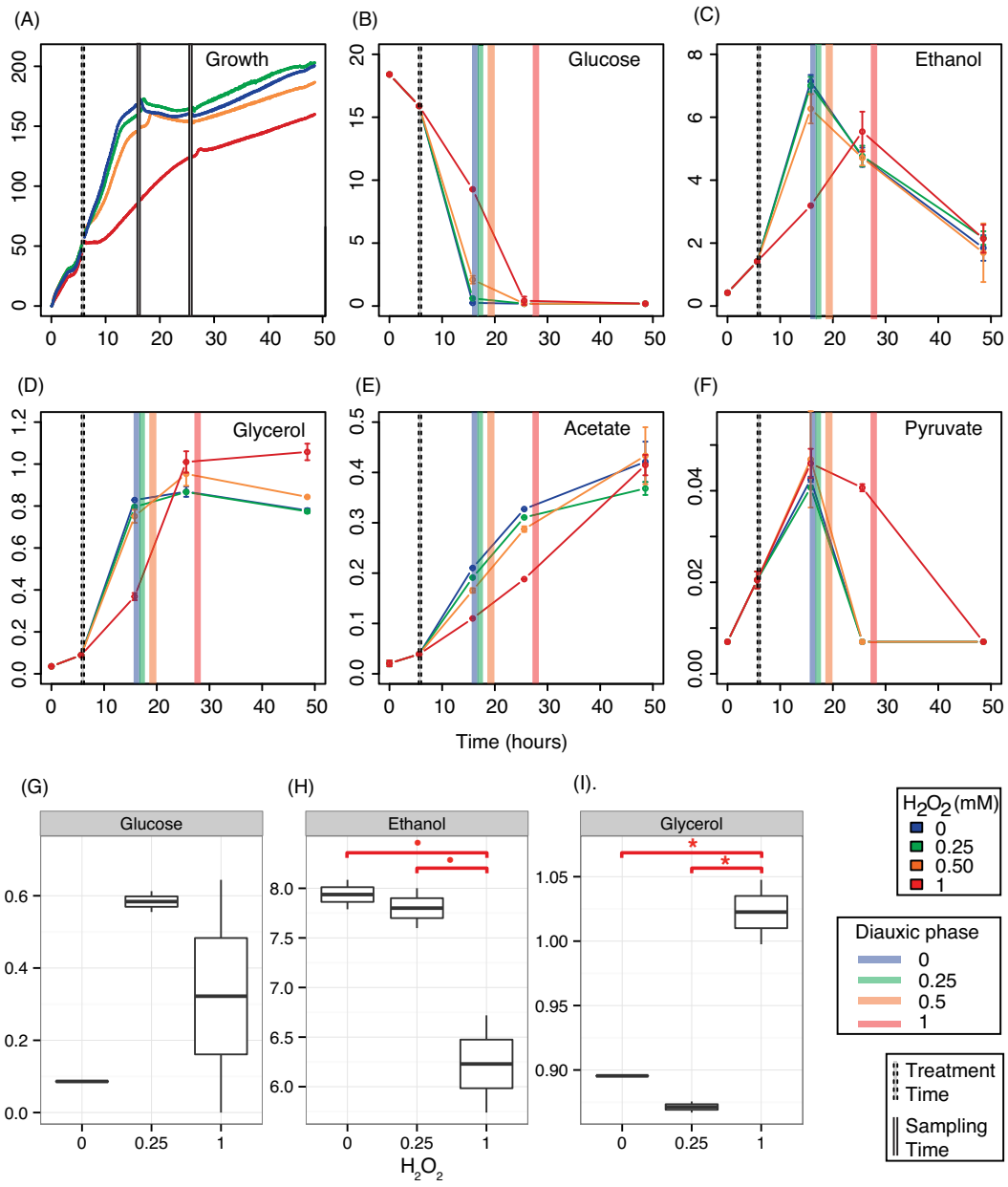

Figure 3. Growth curves and metabolite concentration changes of reference strain *S. cerevisiae* BY4741 under varying oxidative stress conditions. Dashed vertical lines indicate H_2O_2 treatment times, whereas double vertical lines indicate sampling times, y-axis: Scattered light intensity change for biomass (**A**) and metabolite profiles (**B–F**), x-axis: time (hours). Colored vertical bars indicate diauxic phase intervals (B–F). Error bars show standard deviations estimated from replicates. Boxplots of glucose (**G**), ethanol (**H**) and glycerol (**I**) before the diauxic shift time. Red lines indicate the pairwise p-values (* $P < 0.05$, • $P = 0.059$).

Fig. 3G. In this regard, the time point at 15.8 hours for 0, 0.25 and 0.5 mM H_2O_2 treatments and 25.6 hours for 1 mM treatment allowed us to compare the effect of glucose exhaustion on metabolite levels as a function of hydrogen peroxide. Although, the ethanol level observed near the diauxic shift after 1 mM H_2O_2 treatment was nearly significantly different from the control ($p = 0.059$, denoted as •, Fig. 3H), glycerol concentration was significantly increased after 1 mM H_2O_2 treatment compared to 0 and 0.25 mM H_2O_2 treatments (Fig. 3I).

In addition, we simulated the LSU at 620 nm based on the budded fraction of cells versus time data (budding index measure from Brauer *et al.* 2005) using the Rayleigh approximation of Mie scattering (Equation 3). From this simulation (Fig. 2C), we saw that a slow mother–daughter cell separation rate (between 2 and 6 hours) allowed light scattering to follow growth directly, while a rapid cytokinesis rate (between 8 and 10 hours) caused a temporary decrease in predicted LSU (in green). The predicted LSU data was similar to our diauxic shift signature from experimental LSU data (Fig. 2A and B). It should be noted that the aggregate cell volume (purple), representing the total biomass, was increasing throughout the simulation.

Wild-type strains show similar growth physiology compared to non-treatment condition

The mutant strains in our collection were derived from three different but closely related strain backgrounds: BY4741, Y7220 and Y7092 (Fig. 4A-C). It was important to assess whether the

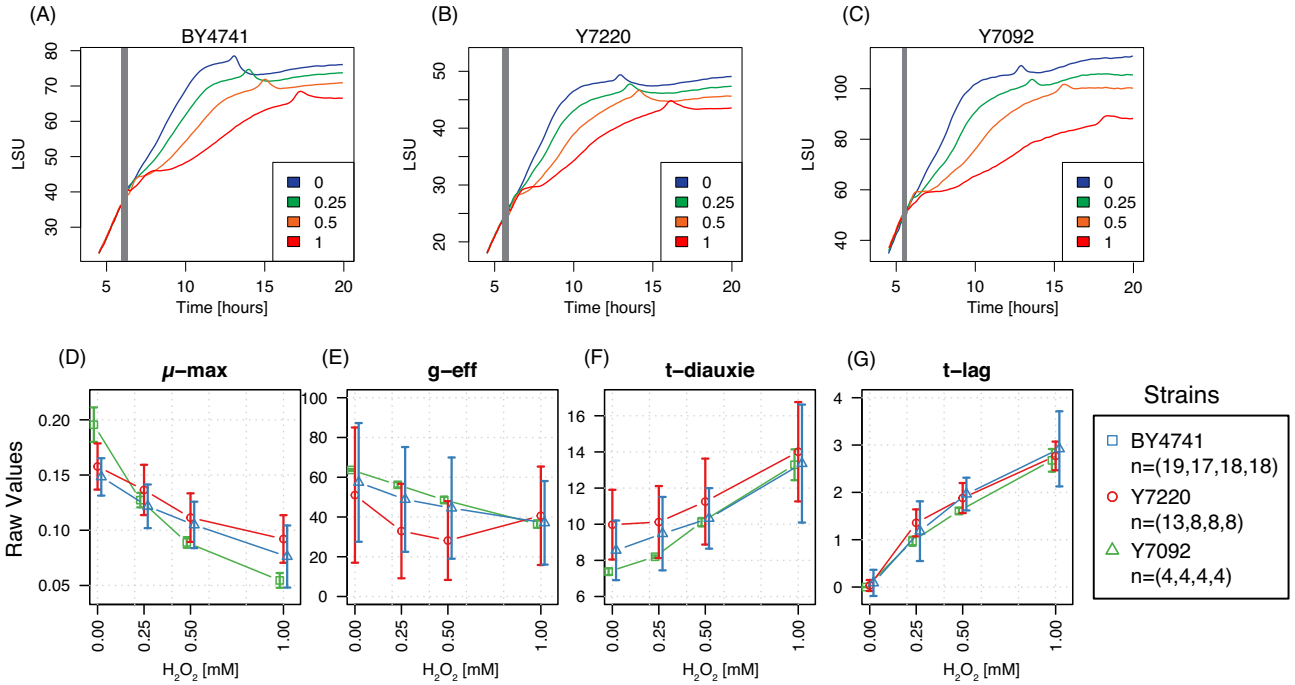

Figure 4. Sample growth curves of background strains and dose response curves for each growth parameter. The background strains BY4741 (**A**), Y7220 (**B**) and Y7092 (**C**) were grown in SD medium and treated with varying concentration of H_2O_2 (mM) as indicated in bottom right legends. Values for growth parameters μ-max (**D**), g-eff (**E**), t-diauxie (**F**) and t-lag (**G**) (non-relative) were calculated for each strain. The bottom right legend shows the background strain information and the number of biological replicates over the different treatment conditions.

individual backgrounds responded differently to H_2O_2 stress in our approach, even though these backgrounds are isogenic and derived from S288c. We therefore tested all three different background strains at different levels of stress and compared the response (Fig. 4).

In agreement with the strains being closely related, we could not identify significant differences in their response to H_2O_2 as measured by the four growth characteristics, except for μ-max of Y7092 vs BY4741 at 0 mM H_2O_2 ($P < 0.004$) (Fig. 4D-F).

Growth parameters describing the oxidative stress response

We next determined the growth curves in the presence of different concentrations of H_2O_2 to induce various levels of oxidative stress. In all cases, the overall shapes of the curves were similar to the one obtained in the absence of H_2O_2 (see Fig. 1D). Importantly, they all showed a diauxic phase signature. However, the timing of this signature was a function of peroxide and the deletion strain. In general, this was also observed for the other parameters extracted from the growth profiles and, as such, described an oxidative stress response, see Fig. 1E. Increasing H_2O_2 concentrations tended to reduce the maximum growth rates (μ-max Fig. 1E-1), increase the length of the lag phase (t-lag, Fig. 1E-2), reduce the growth efficiency after treatment (Fig. 1E-3) and increase the time to onset of the diauxic phase relative to the time point where H_2O_2 was added to the culture (t-diauxie, Fig. 1E-4).

We further tested the significance of each parameter per strain to identify which parameter affects the sensitivity or resistance profile of a strain under oxidative stress. The resulting number of significant strains ($P < 0.05$) was 18 for μ-max, 17 for g-eff, 18 for t-diauxie and 2 for t-lag (see Fig. 5) of the 41 strains. Therefore, approximately half of the strains showed significant effects for the knockout and treatment combination (except for t-lag). Similarly, there were 2, 18, 5 and 0 significant strains for μ-max, g-eff, t-diauxie and t-lag, respectively, in the MMS response. Together with these findings, it can be interpreted that g-eff was the most potent growth parameter value to resolve the fitness profile while it was followed by μ-max and t-diauxie. T-lag, however, had the least impact for the determination of a fitness profile.

After calculating these four growth parameters for all mutant strains, the data were clustered hierarchically to investigate the similarity of oxidative stress as well as DNA damage response between these kinase and phosphatase mutants.

Hierarchical clusters for identification of H_2O_2 sensitivity profiles

The hierarchical clusters based on the four growth parameters based on t-statistics were generated to investigate the patterns of different kinase/phosphatase knockouts. All knockouts and background strains showed similar significant peroxide affects relative to no-treatment controls, e.g. μ-max and g-eff were decreasing while t-diauxie and t-lag were increasing with increasing concentrations of H_2O_2 treatment (data not shown). To understand the importance of the protein kinase or phosphatase, we determined the fitness relative to their strain background and no-treatment control (Fig. 5). The background and treatment controlled relative values, i.e. measurements where strain background and no-treatment control were subtracted, also reflected the t-statistic for the interaction term of the linear model.

Cluster analysis of background and treatment controlled relative values, representing the combination of oxidative stress and gene knockout, resulted in three main clusters of

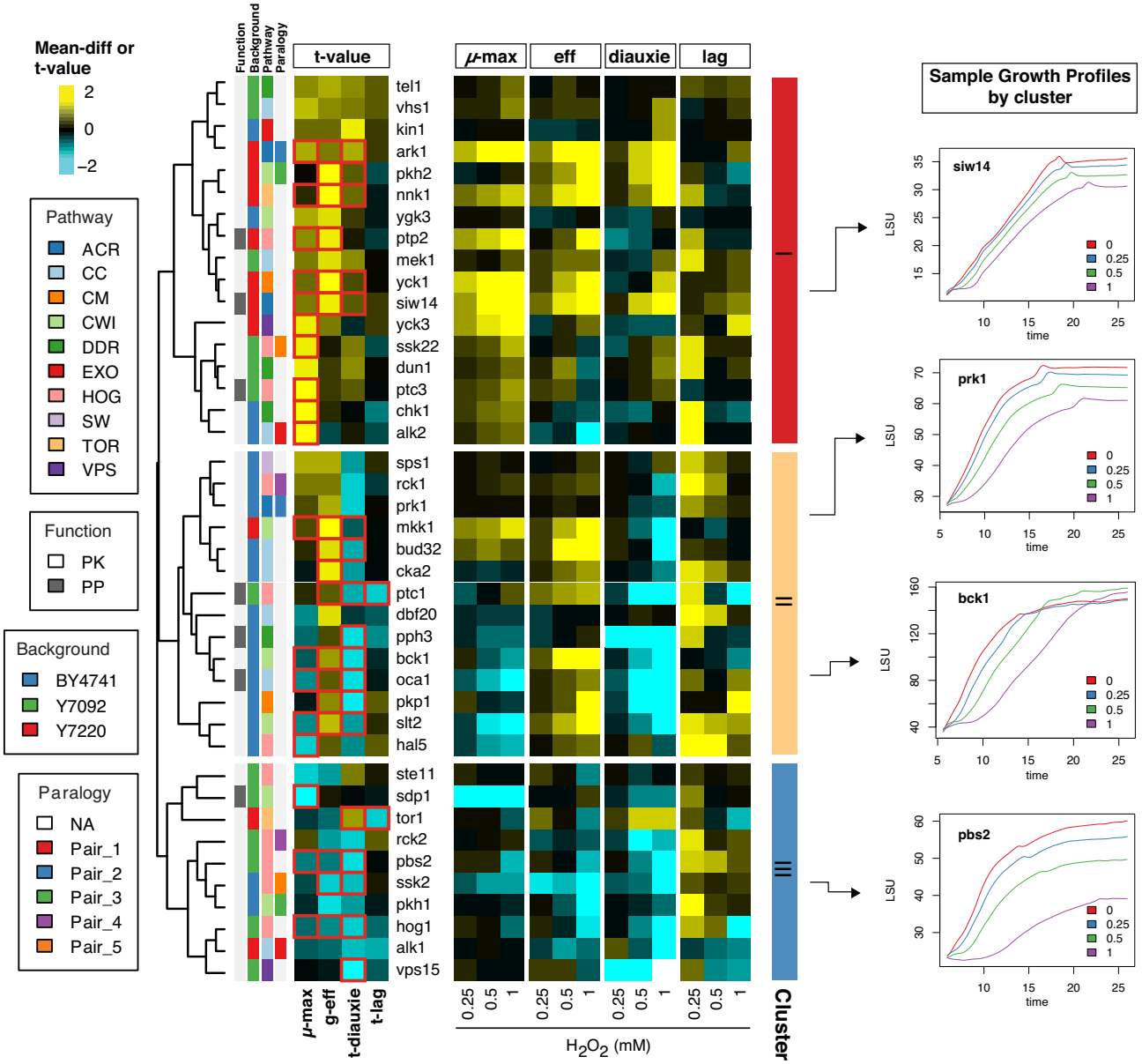

Figure 5. Hierarchical clustering of relative growth parameters for oxidative stress response. Scaled t-values represent the resistance (yellow) or sensitivity (blue) of each growth parameter per strain based on values relative to both strain background and treatment control. Red borders indicate significant t-values ($P < 0.05$). The right heatmap was arranged in three-column groups (0.25, 0.5 and 1 mM H_2O_2) and shows μ-max, g-eff, t-diauxie and t-lag groups relative to background and treatment control. The smaller color-matrix at left of the dendrogram shows the attributes of each strain: 'Pathway' the knockout is involved in; the kinase/phosphatase 'Function'; the 'Background' reference strain and the 'Paralog' group if applicable. Pathway acronyms: ACR, actin cytoskeleton regulation; CC, cell cycle control; CM, carbon metabolism; CWI, cell wall integrity; DDR, DNA damage response; EXO, exocytosis regulation; HOG, high osmolarity glycerol; SW, spore wall biogenesis; TOR, target of rapamycin; VPS, vacuolar protein sorting. In paralog legends, 'NA' stands for not available. Clusters I, II and III were ordered from resistant to sensitive (see the text for the detailed information about the clusters). Sample growth curves of individual knockout strains are shown in the right panel as a representative of each cluster.

knockouts that varied from resistant (cluster I) to sensitive (cluster III) against this stress as seen in (Fig. 5). t-values shown in Fig. 5 were estimates of the gene–peroxide interaction effects in the linear model, and thus can be viewed as a summary of dosage effects in the larger heatmap and provides a simplified view of fitness patterns and clusters.

Some knockout genes in our strain collection have paralogous pairs as indicated in Fig. 5. The differences in fitness in paralogous pairs were always due to one of the paralogs having a different mixed phenotype relative to the other paralog and were therefore located in different clusters. For example, SSK22 in cluster I was more resistant compared to its paralogous gene SSK2 in cluster III. This phenomenon was also observed for ALK1-ALK2 paralogs in the same two clusters.

We performed a complementary analysis with all of the strains to assess if the clusters identified in oxidative stress response remain the same under DNA damage stress, especially if the paralogous groups remained in the same order. As seen in Fig. 6A, there were more phenotypic patterns compared to oxidative stress response. However, most of the strains were more sensitive to MMS stress compared to H_2O_2 in the given concentration ranges of MMS (0–0.05%) and H_2O_2 (0–1 mM). We

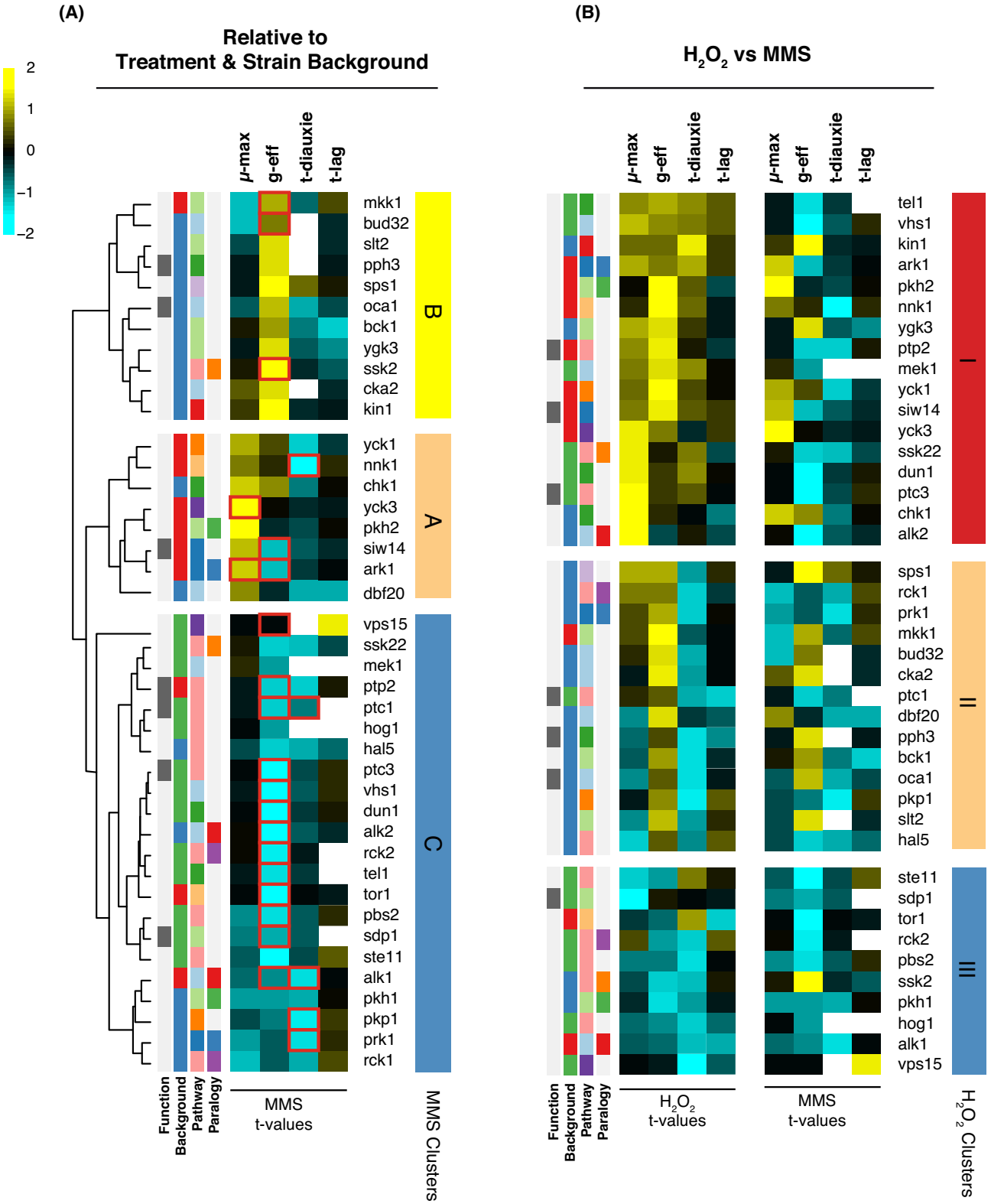

Figure 6. (**A**) Hierarchical clustering of relative growth parameters for DNA damage response. Scaled t-values represent the resistance (yellow) or sensitivity (blue) of each growth parameter per strain based on values relative to background and treatment controls. The red borders of t-values indicate significance ($P < 0.05$). The right heatmap represents 0.05% (v/v) MMS treatment and shows μ-max, g-eff, t-diauxie and t-lag values relative to background and treatment controls, respectively. The color scale and legends are the same as shown in Fig. 5. Clusters were labeled A, B and C from resistant to sensitive, respectively (see the text for the detailed information about the clusters). (**B**) MMS treatment t-values were compared to H_2O_2 treatment t-values. The order of the heatmap follows the same order in Fig. 5.

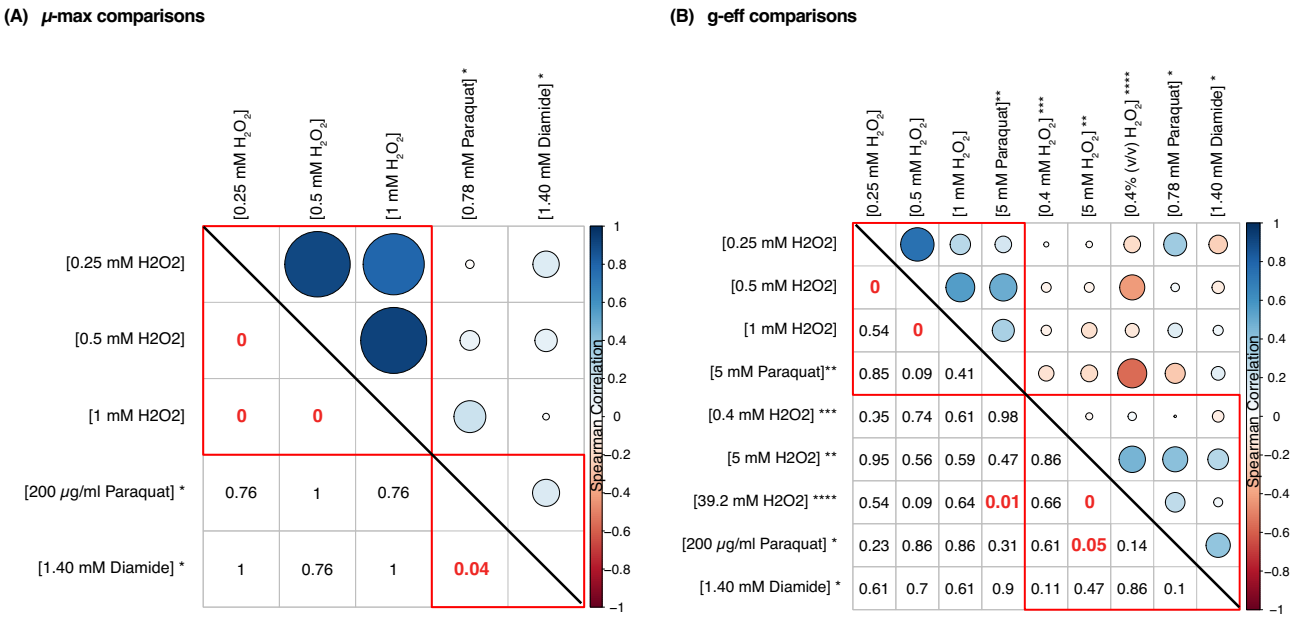

Figure 7. Spearman correlations for μ-max (**A**) and g-eff (**B**) comparisons. The upper and lower parts of the matrix, above or below diagonal border (black), indicate the Spearman correlation coefficient (circle size) and p-values, respectively. The positive correlations are shown in blue and negative correlations are shown in red color scale. Significant p-values are indicated as red. The data taken from different resources are indicated as follows: * (Fernandez-Ricaud *et al.* 2005), **(Hillenmeyer *et al.* 2010), *** (Kelley and Ideker 2009), ****(Parsons *et al.* 2006).

identified clusters of fitness profiles from resistant to sensitive as cluster A to cluster C, respectively. Cluster A displayed the most resistant strains, but the fitness was mixed since t-diauxie and t-lag were mostly sensitive. Cluster B was more sensitive although it showed resistance mainly in g-eff parameter. Clusters C represented the most sensitive groups.

A comparison to available datasets

We compared our H_2O_2 dataset with phenotypes from various high-throughput approaches, including the microarray hybridization-based competitive growth assays (Parsons *et al.* 2006; Kelley and Ideker 2009; Hillenmeyer *et al.* 2010) and high-throughput fermentation data (Fernandez-Ricaud *et al.* 2005). The only growth parameters compared were g-eff and μ-max since there was no diauxic shift datasets. Also, t-lag comparisons were excluded because no analogous stress intervention data existed.

Spearman correlation coefficients were used as a similarity measure for the different data types (Fig. 7). The growth rates (μ-max) represented in this study strongly correlated with each other. Also, paraquat and diamide treatments had a close correlation between each other. Paraquat phenotypes had the largest correlation coefficient with different H_2O_2 treatments although these correlations were not statistically significant.

Identification of paralogous gene knockouts in oxidative stress fitness profiles

Despite the fact that the correlations were not significant, paraquat treatments (Fernandez-Ricaud *et al.* 2005; Hillenmeyer *et al.* 2010) were comparable to our data. Therefore, the high-throughput fermentation data for all protein kinases and phosphatases were retrieved for paralogy comparison over three growth parameters (efficiency, mu-max, lag-time).

There were eight clusters detected in paraquat treatment data (k-means clustering) for all catalytic protein kinases and phosphatases. In Fig. 8, each gene of a paralogous pair was represented in red when found in different clusters (46 strains) or blue if in the same cluster (8 strains). In summary, 85% of paralogous gene pairs displayed different fitness profiles. The same analysis was applied to different stress types profiled in PROPHECY and paralogous counterparts were clustered in different fitness profiles 88%, 60% and 62% for diamide, DTT and NaCl treatments, respectively (Table 1).

Randomized trials suggest that the observed patterns of paralogous pairs would be expected in random cluster of the same size about 14% of the time. Although this observation is clearly not significant, the expectation that paralogous deletions give rise to similar phenotypes was not supported.

DISCUSSION

Diauxic shift detection

Apart from diauxic shift delay (t-diauxie), established methods have existed for measuring the growth attributes: maximum growth rate (μ-max), lag phase duration (t-lag) and growth efficiency (g-eff). Numerous methods are available to track glucose concentrations in media, e.g. enzymatic assays based on glucose oxidase activity (Garreau *et al.* 2000), HPLC isocratic method (Diano *et al.* 2006) and other fluorescent-based glucose sensors (Pickup *et al.* 2005). Although these methods are effective at measuring glucose consumption rates, they are labor intensive, expensive or require genetic modification. In this work, we have proposed a novel method to identify the diauxic shift by using the first derivatives of light-scattering curves generated by a high-throughput microfermentation platform. The agreement between the first derivative method and an HPLC-based metabolite profiling method for detecting the diauxic phase showed that the former was accurate and can be used for more precise diauxic phase detection (Fig. 3).

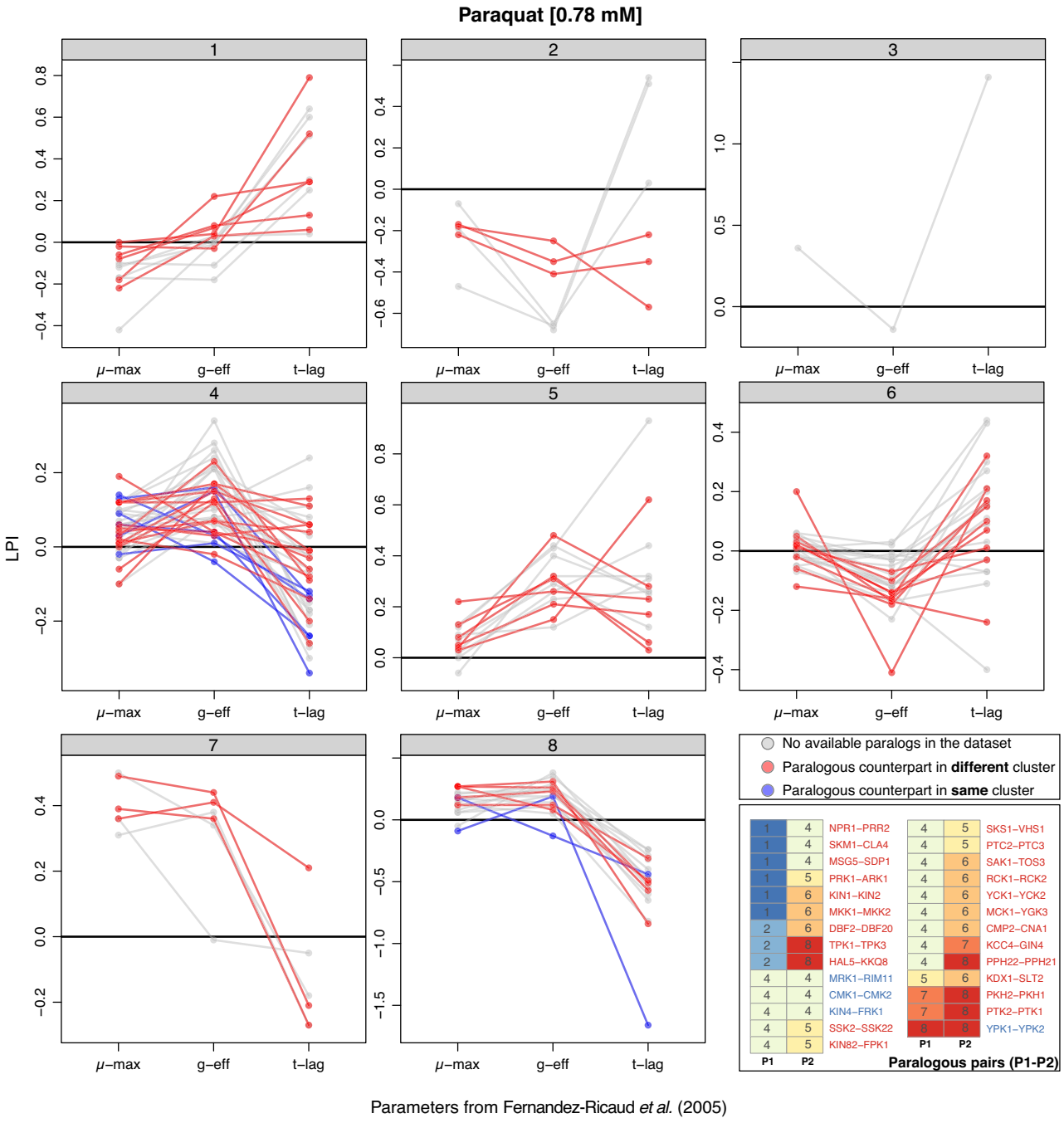

Figure 8. Paraquat fitness data for μ-max, g-eff and t-lag. Each panel shows a k-means cluster. The resistance (above zero) and sensitivity (below zero) are defined as LPI values (Warringer *et al.* 2003). The knockouts without paralogs are indicated with gray lines. The knockouts that have a paralogous counterpart in the same or different cluster are shown in blue or red, respectively. The panel at the right bottom shows the cluster distribution of each knockout and its paralogous counterpart.

Oxidative stress response on central carbon metabolism

Saccharomyces cerevisiae, as a Crabtree-positive microorganism, prefers to utilize glucose via fermentative pathway in excess glucose conditions as used here. When considering the regulation of the diauxic shift and its dependence on carbon utilization, it is important to consider that yeast cells use both aerobic respiration (oxidative phosphorylation) and anaerobic respiration (alcoholic fermentation) during exponential growth (Hohmann and Mager 2003).

Glycerol production increases exponentially until the population reaches the diauxic shift (Zhang, Olsson and Nielsen 2010; Zampar *et al.* 2013) and it is consumed after the diauxic shift. Moreoever, glycerol production is triggered via the HOG pathway under osmotic stress conditions, but not only as a response to osmotic stress (Hohmann 2009). It was found that yeast cells exposed to H_2O_2 must increase the glycerol synthesis due to increased levels of glycerol phosphate dehydrogenase (Gpd1p) and glycerol phosphate phosphatase (Gpp2p) (Godon *et al.* 1998). Another important finding from Godon *et al.* (1998) was the redirection of carbon fluxes to favor the NADPH regeneration by

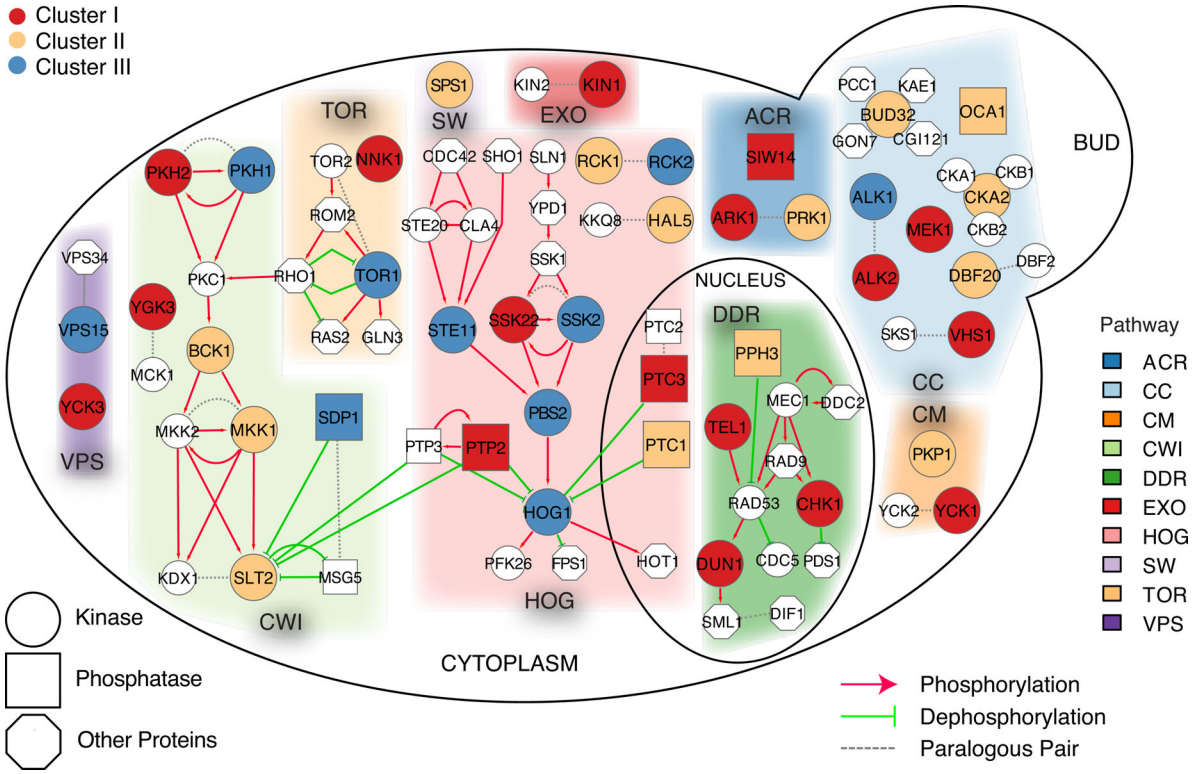

Figure 9. Integrated view of protein kinase/phosphatase network for oxidative stress signaling. The directionality of the network is retrieved from the literature and the colors of the nodes and acronyms for networks are implemented from Fig. 5. Genes that were not studied are implicated as smaller white nodes.

Table 1. The effect of different environmental stress on paralogous genes.

Environment	Number of clusters	Paralog pairs	Paralog pairs in same cluster	Empirical p-value
H_2O_2 [a][0.25, 0.5, 1 mM]	3	5	0	0.14
MMS [a][0.05% (v/v)]	3	5	2	0.71
Diamide [b][1.40 mM]	8	25	3	0.32
Paraquat [b][0.78 mM]	8	27	4	0.38
DTT [b][1.60 mM]	8	15	6	0.97
NaCl [b][0.85 M]	8	27	10	0.99

[a]Hierarchical clusters (this study), [b]k-means clusters (Fernandez-Ricaud *et al.* 2005).

repression of glycolysis. The regeneration of NADPH pool is crucial for the recovery from oxidative damage since it is essential for the activity of thioredoxin system and glutathione/glutaredoxin system (Holmgren 1989). Also, strains lacking both glycerol 3-phosphatases (*gpp1*Δ *gpp2*Δ), enzymes with functions that are essential for glycerol synthesis, were hypersensitive to oxidative stress (Påhlman *et al.* 2001).

Our observations showed that glycerol was also produced under oxidative stress (Fig. 3). The increase in glycerol and decrease in ethanol levels are consistent with the previous findings and indicate that metabolism has been redirected to glycerol production. This results in a dosage-dependent reduction in rate of carbon utilization for growth and provides a distinct phenotypic profile to characterize the oxidative stress of a strain.

Phenotypic profiles differ by concentration of the oxidizing agent

The μ-max and g-eff in this study were subject to comparison to literature data. The variation of both growth parameters in this study was not high; therefore, the correlations between 0.25 mM and 0.5 mM as well as between 0.5 mM and 1 mM H_2O_2 treatments were significant for both μ-max and g-eff. Comparison of μ-max to the paraquat data set in PROPHECY (Fernandez-Ricaud *et al.* 2005) did not show a high correlation possibly due to the difference in oxidizing agents. For example, H_2O_2 acts on the generation of hydroxyl radical, while paraquat triggers the formation of superoxide (Morano, Grant and Moye-Rowley 2012). Also, the physical conditions such as fermentation volume and shaking speed effect the phenotypic responses.

In addition to the PROHECY data sets, microarray hybridization-based competitive growth assay (chemical genetic profiling) data were compared to our g-eff measurements. Positive correlations were only observed for paraquat treatments from both Fernandez-Ricaud *et al.* (2005) and Hillenmeyer *et al.* (2010) to our g-eff data. Thus, the data from Fernandez-Ricaud *et al.* (2005) were used for the paralogous pair comparison whether there were different fitness profiles of these genes.

Paralogs display different growth profiles

A number of protein kinases in this study have paralogs although the profiles of paralog pairs tended to be different and were observed in different clusters under both oxidative and DNA damage stress (Figs 5 and 6). This observation argues that paralogous genes do not have clear compensatory function and do not represent simple evolutionary redundancy. Li, Yuan and Zhang (2010) also observed this phenomenon as most of the paralog duplicates lost their compensatory activity in environmental responses. Contrastingly, it was found that the *ARK1-PRK1* paralogous pair displayed only small effects in gene expression in either knockout alone, suggesting redundant functional roles (van Wageningen *et al.* 2010). However, we found that these knockouts showed different phenotypic profiles (e.g. cluster I–cluster III, respectively) when challenged with oxidative stress implying functional specialization. This only suggests that the phenotypic difference in stress response may not be reflected in the gene expression patterns of knockouts in non-stress conditions, i.e. genetic effects are not the same as environmental responses. This underlines the importance of our approach where both genetic and environmental factors are considered together to implicate a functional role of a gene in oxidative stress.

In addition, the phenotypic responses of paralogous protein kinases varied depending on the stress condition (Fig. 6B) when comparing MMS to H_2O_2 stress. Paralogous kinase pairs made up a quarter of the strains we investigated (10/41) and are likely representative of kinase paralogs in general. Interestingly, paralogous kinases knockouts Δ*alk1* and Δ*alk2* were both sensitive to MMS (cluster C), while Δ*alk1* was sensitive and Δ*alk2* was resistant in response to H_2O_2 stress (cluster III–cluster I, respectively). *ALK2* is considered to be an important gene for cell cycle regulation, and unlike *ALK1*, overexpression of *ALK2* caused cell cycle arrest (Nespoli *et al.* 2006). Our analysis also supports that both *ALK1* and *ALK2* are important in DNA damage stress (Nespoli *et al.* 2006) since Δ*alk1* and Δ*alk2* were sensitive to MMS treatment.

To investigate whether this trend generalized to larger sets of paralogous pairs, the paraquat treatment data (Fernandez-Ricaud *et al.* 2005) was investigated for all PK/PP deletions available in the dataset. Since the μ-max and g-eff data were correlated with the effects of the oxidizing agent paraquat (although not significantly), further analyses were performed using the paraquat series to estimate whether paralogous pairs resulted in similar or different fitness patterns. The extent of dissimilarity between paralogous pairs, where 85% of pairs were assigned to different fitness groups, was similar to our findings (Fig. 8).

Although the evolutionary retention of paralogous pairs could provide functional overlap and increased gene dosage affects, here we did not observe compensation for any paralogous pair in either stress responses (Figs 5 and 6). We observed members of paralogous pairs in different clusters of phenotypic traits implying the different functional roles for those genes against stress responses except Δ*alk1*-Δ*alk2* and Δ*rck1*-Δ*rck2* in MMS response. Most often, one individual of a pair displayed high sensitivity compared to the other individual. Again, this was true for both stress responses. For example, in response to oxidative stress, individuals from four paralogs pairs can be observed in cluster III (Δ*alk1*, Δ*pkh1*, Δ*rck2* and Δ*ssk2* in Fig. 5), the most sensitive cluster, while their paralogous members were observed in more resistant clusters. Similarly, in response to MMS, paralog members were again grouped in the most sensitive cluster (Δ*pkh1*, Δ*prk1* and Δ*ssk22* in Fig. 6, cluster C) where their paralogs were found in more resistant clusters. One explanation for different phenotypes of paralogs pairs is this lack or evolutionary retention for compensatory paralogs as such paralogs are dispensable.

The reason why some mutants exhibit both resistance and sensitivity might be explained in the context of antagonistic pleiotropy, which is defined as the fitness trade-off among the phenotypic traits controlled by one gene or locus. For example, the strains in cluster II (Fig. 5) displayed sensitivity by t-diauxie trait while showing resistance by the g-eff trait. Also, these observations were statistically significant at least for half of the strains in these growth parameters. This phenotypic trade-off could be interpreted as an evolutionary strategy for acquiring resistance to environmental stress and may suggest how parologous genes evolve to have opposing phenotypes.

Final characterization of oxidative stress sensitivity and resistance

Analysis of fitness relative to both strain background and treatment control best illustrated the combined influence of genetic and environmental response to varying oxidative stress and DNA damage conditions (Figs 5 and 6). By using the relative phenotypes, we have identified five main clusters in both oxidative and DNA damage stress based on strain phenotype profiles.

For an overview of the cell signaling networks in yeast, the genome-wide protein kinase/phosphatase networks were compiled from the literature (Harrison and Haber 2006; Hohmann, Krantz and Nordlander 2007; O'Neill *et al.* 2007; Levin 2011; Baltanas *et al.* 2013) as shown in Fig. 9. This integrated view also showed the interplay between TOR, CWI and HOG signaling.

Knocking out transcription effector kinases that regulate the gene expression directly, Δ*slt2* and Δ*hog1*, or cutting the signal transduction to these kinases by knocking out, e.g. Δ*pbs2*, were found to cause very defective phenotypes. This confirms the importance of these protein kinases and phosphatases in the oxidative stress response. When one of the connections between HOG and CWI is cut, e.g. by knocking out phosphatase Δ*ptp2*, the cell becomes more resistant to oxidative stress suggesting that cells were pre-adapted as there was diminished phosphatase activity to downregulate the activity of *SLT2* and *HOG1* by dephosphorylation. The same phenomenon appeared to apply to Δ*ptc3* as well.

The HOG pathway appeared to have many different epistatic relationships with other important kinase/phosphatase pathways. In agreement with the previous studies (Bilsland *et al.* 2004; Ikner and Shiozaki 2005), we found that the HOG pathway was very important for recover from the damaging effects of oxidative stress. Half of the HOG pathway null mutants were found in sensitive clusters, 5 of 11 in cluster III.

Multivariate phenotypic screens, as represented in this work, could be used to provide information on engineering oxidative stress-resistant strains. Certainly, there are many applications where oxidative stress-resistant strains would be advantageous in a biotechnology setting, or to gain a better understanding of how environmental stresses influence aging and cancer progression.

One engineering strategy for oxidative stress-resistant strains would be the overexpression of the sensitive genes. However, an overexpression strategy would likely require careful induction or a titratable promoter due to the possible lethality issues caused by overexpression. For example, *HOG1* overexpression did not cause toxicity while *PBS2* overexpression was lethal (Krantz *et al.* 2009), although *PBS2* lethality was suppressed by *SSK2* deletion in the same strain (Hohmann 2009). Another strat-

egy would be the double or multiple deletions of the resistant knockout strains. Clearly, cluster I genes are good candidates for this approach. Among all, the kinases regulating the upstream signaling network of effector kinases (e.g. Δ*pkh2*, Δ*sdp1*, Δ*ste11*) or the phosphatases that are deregulating the effector kinases (e.g. Δ*ptp2*, Δ*ptc3*) would be the best candidates. In addition, our strategy may prove useful for functional phenotypic studies of heterologously expressed proteins with unknown functions.

In summary, we successfully characterized complex phenotypic patterns of protein kinase and phosphatase knockouts and highlighted the important role of Hog1p and associated pathway proteins in oxidative stress response. Knockouts resulting in improved relative fitness may represent the generation of pre-adapted cells and the pattern of fitness may implicate more specifically why this is so.

SUPPLEMENTARY DATA

Supplementary data are available at FEMSYR online.

ACKNOWLEDGEMENTS

We would like to thank Jesper Mogensen for his very kind help with the HPLC experiments, and Mhairi Workman for her valuable scientific comments and proofreading of this manuscript. Thanks to Ruedi Abersold, Matthias Peter, Bernd Bodenmiller and Claudine Kraft for providing yeast strains.

FUNDING

This work was supported by European Commission grant FP7 UNICELLSYS (ref. no. 201142).

Conflict of interest. None declared.

REFERENCES

Ames BN, Shigenaga MK, Hagen TM. Oxidants, antioxidants, and the degenerative diseases of aging. *P Natl Acad Sci USA* 1993;**90**:7915–22.

Avery AM, Avery SV. *Saccharomyces cerevisiae* expresses three phospholipid hydroperoxide glutathione peroxidases. *J Biol Chem* 2001;**276**:33730–5.

Baltanas R, Bush A, Couto A, *et al*. Pheromone-induced morphogenesis improves osmoadaptation capacity by activating the HOG MAPK pathway. *Sci Signal* 2013;**6**: ra26.

Benjamini Y, Hochberg Y. Controlling the false discovery rate: a practical and powerful approach to multiple testing. *J Roy Stat Soc B Met* 1995;**57**:289–300.

Bilsland E, Molin C, Swaminathan S, *et al*. Rck1 and Rck2 MAPKAP kinases and the HOG pathway are required for oxidative stress resistance. *Mol Microbiol* 2004;**53**:1743–56.

Blomberg A. Measuring growth rate in high-throughput growth phenotyping. *Curr Opin Biotechnol* 2011;**22**:94–102.

Bodenmiller B, Wanka S, Kraft C, *et al*. Phosphoproteomic analysis reveals interconnected system-wide responses to perturbations of kinases and phosphatases in yeast. *Sci Signal* 2010;**3**:rs4.

Brauer MJ, Huttenhower C, Airoldi EM, *et al*. Coordination of growth rate, cell cycle, stress response, and metabolic activity in yeast. *Mol Biol Cell* 2008;**19**:352–67.

Brauer MJ, Saldanha AJ, Dolinski K, *et al*. Homeostatic adjustment and metabolic remodeling in glucose-limited yeast cultures. *Mol Biol Cell* 2005;**16**:2503–17.

Breitkreutz A, Choi H, Sharom JR, *et al*. A global protein kinase and phosphatase interaction network in yeast. *Science* 2010;**328**:1043–6.

Cherry JM, Hong EL, Amundsen C, *et al*. Saccharomyces Genome Database: the genomics resource of budding yeast. *Nucleic Acids Res* 2012;**40**:D700–5.

Cooke MS, Evans MD, Dizdaroglu M, *et al*. Oxidative DNA damage: mechanisms, mutation, and disease. *FASEB J* 2003;**17**:1195–214.

Cox A, DeWeerd AJ, Linden J. An experiment to measure Mie and Rayleigh total scattering cross sections. *Am J Phys* 2002;**70**:620–5.

De Deken RH. The Crabtree effect: a regulatory system in yeast. *J Gen Microbiol* 1966;**44**:149–56.

Diano A, Bekker-Jensen S, Dynesen J, *et al*. Polyol synthesis in *Aspergillus niger*: influence of oxygen availability, carbon and nitrogen sources on the metabolism. *Biotechnol Bioeng* 2006;**94**:899–908.

Eisen MB, Spellman PT, Brown PO, *et al*. Cluster analysis and display of genome-wide expression patterns. *P Natl Acad Sci USA* 1998;**95**:14863–8.

Farrugia G, Balzan R. Oxidative stress and programmed cell death in yeast. *Front Oncol* 2012;**2**:64.

Fernandez-Ricaud L, Warringer J, Ericson E, *et al*. PROPHECY-a database for high-resolution phenomics. *Nucleic Acids Res* 2005;**33**:D369–73.

Garreau H, Hasan RN, Renault G, *et al*. Hyperphosphorylation of Msn2p and Msn4p in response to heat shock and the diauxic shift is inhibited by cAMP in Saccharomyces cerevisiae. *Microbiology* 2000;**146**(Pt 9):2113–20.

Gasch AP, Spellman PT, Kao CM, *et al*. Genomic expression programs in the response of yeast cells to environmental changes. *Mol Biol Cell* 2000;**11**:4241–57.

Godon C, Lagniel G, Lee J, *et al*. The H2O2 Stimulon in *Saccharomyces cerevisiae*. *J Biol Chem* 1998;**273**:22480–9.

Halliwell B. Antioxidants and human disease: a general introduction. *Nutr Rev* 1997;**55**:S44–9; discussion S49–52.

Harrison JC, Haber JE. Surviving the breakup: the DNA damage checkpoint. *Annu Rev Genet* 2006;**40**:209–35.

Herdeiro RS, Pereira MD, Panek AD, *et al*. Trehalose protects *Saccharomyces cerevisiae* from lipid peroxidation during oxidative stress. *Biochim Biophys Acta* 2006;**1760**:340–6.

Hillenmeyer ME, Ericson E, Davis RW, *et al*. Systematic analysis of genome-wide fitness data in yeast reveals novel gene function and drug action. *Genome Biol* 2010;**11**:R30.

Hohmann S. Control of high osmolarity signalling in the yeast *Saccharomyces cerevisiae*. *FEBS Lett* 2009;**583**:4025–9.

Hohmann S, Krantz M, Nordlander B. Yeast osmoregulation. *Methods Enzymol* 2007;**428**:29–45.

Hohmann S, Mager WH. Yeast Stress Responses. *Topics in Current Genetics* 2003:**1**.

Holmgren A. Thioredoxin and glutaredoxin systems. *J Biol Chem* 1989;**264**:13963–6.

Howlett NG, Avery SV. Induction of lipid peroxidation during heavy metal stress in Saccharomyces cerevisiae and influence of plasma membrane fatty acid unsaturation. *Appl Environ Microb* 1997;**63**:2971–6.

Huang ME, Kolodner RD. A biological network in *Saccharomyces cerevisiae* prevents the deleterious effects of endogenous oxidative DNA damage. *Mol Cell* 2005;**17**:709–20.

Huang ME, Rio AG, Nicolas A, *et al*. A genomewide screen in *Saccharomyces cerevisiae* for genes that suppress the accumulation of mutations. *P Natl Acad Sci USA* 2003;**100**: 11529–34.

Ikner A, Shiozaki K. Yeast signaling pathways in the oxidative stress response. *Mutat Res* 2005;**569**:13–27.

Jamieson DJ. *Saccharomyces cerevisiae* has distinct adaptive responses to both hydrogen peroxide and menadione. *J Bacteriol* 1992;**174**:6678–81.

Jamieson DJ. Oxidative stress responses of the yeast *Saccharomyces cerevisiae*. *Yeast* 1998;**14**:1511–27.

Jombart T. adegenet: a R package for the multivariate analysis of genetic markers. *Bioinformatics* 2008;**24**:1403–5.

Kelley R, Ideker T. Genome-wide fitness and expression profiling implicate Mga2 in adaptation to hydrogen peroxide. *PLoS Genet* 2009;**5**:e1000488.

Kitanovic A, Wolfl S. Fructose-1,6-bisphosphatase mediates cellular responses to DNA damage and aging in *Saccharomyces cerevisiae*. *Mutat Res* 2006;**594**:135–47.

Krantz M, Ahmadpour D, Ottosson LG, *et al.* Robustness and fragility in the yeast high osmolarity glycerol (HOG) signal-transduction pathway. *Mol Syst Biol* 2009;**5**:281.

Landolfo S, Zara G, Zara S, *et al.* Oleic acid and ergosterol supplementation mitigates oxidative stress in wine strains of *Saccharomyces cerevisiae*. *Int J Food Microbiol* 2010;**141**:229–35.

Levin DE. Regulation of cell wall biogenesis in *Saccharomyces cerevisiae*: the cell wall integrity signaling pathway. *Genetics* 2011;**189**:1145–75.

Li J, Yuan Z, Zhang Z. The cellular robustness by genetic redundancy in budding yeast. *PLoS Genet* 2010;**6**:e1001187.

Monod J. The growth of bacterial cultures. *Annu Rev Microbiol* 1949;**3**:371–94.

Morano KA, Grant CM, Moye-Rowley WS. The response to heat shock and oxidative stress in *Saccharomyces cerevisiae*. *Genetics* 2012;**190**:1157–95.

Nespoli A, Vercillo R, di Nola L, *et al.* Alk1 and Alk2 are two new cell cycle-regulated haspin-like proteins in budding yeast. *Cell Cycle* 2006;**5**:1464–71.

Ng CH, Tan SX, Perrone GG, *et al.* Adaptation to hydrogen peroxide in *Saccharomyces cerevisiae*: the role of NADPH-generating systems and the SKN7 transcription factor. *Free Radical Bio Med* 2008;**44**:1131–45.

Nystrom T. Role of oxidative carbonylation in protein quality control and senescence. *EMBO J* 2005;**24**:1311–7.

O'Neill BM, Szyjka SJ, Lis ET, *et al.* Pph3-Psy2 is a phosphatase complex required for Rad53 dephosphorylation and replication fork restart during recovery from DNA damage. *P Natl Acad Sci USA* 2007;**104**:9290–5.

Osorio H, Moradas-Ferreira P, Gunther Sillero MA, *et al.* In *Saccharomyces cerevisiae*, the effect of H2O2 on ATP, but not on glyceraldehyde-3-phosphate dehydrogenase, depends on the glucose concentration. *Arch Microbiol* 2004;**181**:231–6.

Påhlman A-K, Granath K, Ansell R, *et al.* The yeast glycerol 3-phosphatases Gpp1p and Gpp2p are required for glycerol biosynthesis and differentially involved in the cellular responses to osmotic, anaerobic, and oxidative stress. *J Biol Chem* 2001;**276**:3555–63.

Parsons AB, Lopez A, Givoni IE, *et al.* Exploring the mode-of-action of bioactive compounds by chemical-genetic profiling in yeast. *Cell* 2006;**126**:611–25.

Paumi CM, Pickin KA, Jarrar R, *et al.* Ycf1p attenuates basal level oxidative stress response in *Saccharomyces cerevisiae*. *FEBS Lett* 2012;**586**:847–53.

Perrone GG, Tan SX, Dawes IW. Reactive oxygen species and yeast apoptosis. *Biochim Biophys Acta* 2008;**1783**:1354–68.

Pickup JC, Hussain F, Evans ND, *et al.* Fluorescence-based glucose sensors. *Biosens Bioelectron* 2005;**20**:2555–65.

Pons M-N, Rajab A, Engasser J-M. Influence of acetate on growth kinetics and production control of Saccharomyces cerevisiae on glucose and ethanol. *Appl Microbiol Biot* 1986;**24**:193–8.

Saghbini M, Hoekstra D, Gautsch J. Media formulations for various two-hybrid systems (Two-Hybrid Systems). *Methods in Molecular Biology* 2001;**177**:15–39.

Salmon TB, Evert BA, Song B, *et al.* Biological consequences of oxidative stress-induced DNA damage in Saccharomyces cerevisiae. *Nucleic Acids Res* 2004;**32**:3712–23.

Singh KK. The *Saccharomyces cerevisiae* Sln1p-Ssk1p two-component system mediates response to oxidative stress and in an oxidant-specific fashion. *Free Radical Bio Med* 2000;**29**:1043–50.

Singh KK, Sigala B, Sikder HA, *et al.* Inactivation of Saccharomyces cerevisiae OGG1 DNA repair gene leads to an increased frequency of mitochondrial mutants. *Nucleic Acids Res* 2001;**29**:1381–8.

Temple MD, Perrone GG, Dawes IW. Complex cellular responses to reactive oxygen species. *Trends Cell Biol* 2005;**15**:319–26.

van Loon B, Markkanen E, Hubscher U. Oxygen as a friend and enemy: How to combat the mutational potential of 8-oxoguanine. *DNA Repair* 2010;**9**:604–16.

van Wageningen S, Kemmeren P, Lijnzaad P, *et al.* Functional overlap and regulatory links shape genetic interactions between signaling pathways. *Cell* 2010;**143**:991–1004.

Warringer J, Ericson E, Fernandez L, *et al.* High-resolution yeast phenomics resolves different physiological features in the saline response. *P Natl Acad Sci USA* 2003;**100**:15724–9.

Winderickx J, Holsbeeks I, Lagatie O, *et al.* From feast to famine; adaptation to nutrient availability in yeast (Yeast Stress Responses). *Topics in Current Genetics* 2003;**1**:305–86.

Zampar GG, Kümmel A, Ewald J, *et al.* Temporal system-level organization of the switch from glycolytic to gluconeogenic operation in yeast. *Mol Syst Biol* 2013;**9**:1–13.

Zhang J, Olsson L, Nielsen J. The β-subunits of the Snf1 kinase in *Saccharomyces cerevisiae*, Gal83 and Sip2, but not Sip1, are redundant in glucose derepression and regulation of sterol biosynthesis. *Mol Microbiol* 2010;**77**:371–83.

Zong WX, Ditsworth D, Bauer DE, *et al.* Alkylating DNA damage stimulates a regulated form of necrotic cell death. *Gene Dev* 2004;**18**:1272–82.